Influence of Collector Surface Composition and Water Chemistry on the Deposition of Cerium Dioxide Nanoparticles: QCM-D and Column Experiment Approaches

ARTICLE *in* ENVIRONMENTAL SCIENCE & TECHNOLOGY · MAY 2012

Impact Factor: 5.33 · DOI: 10.1021/es300883q · Source: PubMed

3 AUTHORS:

Xuyang Liu
United States Environmental Protection Agency
12 PUBLICATIONS **405** CITATIONS
SEE PROFILE

Gexin Chen
United States Environmental Protection Agency
17 PUBLICATIONS **393** CITATIONS
SEE PROFILE

Chunming Su
United States Environmental Protection Agency
53 PUBLICATIONS **2,267** CITATIONS
SEE PROFILE

Environmental Science & Technology

Article

pubs.acs.org/est

Influence of Collector Surface Composition and Water Chemistry on the Deposition of Cerium Dioxide Nanoparticles: QCM-D and Column Experiment Approaches

Xuyang Liu,[†,*] Gexin Chen,[†] and Chunming Su[‡,*]

[†]National Research Council Resident Research Associate, U.S. Environmental Protection Agency, 919 Kerr Research Drive, Ada, Oklahoma 74820, United States

[‡]Ground Water and Ecosystems Restoration Division, National Risk Management Research Laboratory, Office of Research and Development, U.S. Environmental Protection Agency, 919 Kerr Research Drive, Ada, Oklahoma 74820, United States

Supporting Information

ABSTRACT: The deposition behavior of cerium dioxide (CeO_2) nanoparticles (NPs) in dilute NaCl solutions was investigated as a function of collector surface composition, pH, ionic strength, and organic matter (OM). Sensors coated separately with silica, iron oxide, and alumina were applied in quartz crystal microbalance with dissipation (QCM-D) to examine the effect of these mineral phases on CeO_2 deposition in NaCl solution (1−200 mM). Frequency and dissipation shift followed the order: silica > iron oxide > alumina in 10 mM NaCl at pH 4.0. No significant deposition was observed at pH 6.0 and 8.5 on any of the tested sensors. However, ≥ 94.3% of CeO_2 NPs deposited onto Ottawa sand in columns in 10 mM NaCl at pH 6.0 and 8.5. The inconsistency in the different experimental approaches can be mainly attributed to NP aggregation, surface heterogeneity of Ottawa sand, and flow geometry. In QCM-D experiments, the deposition kinetics was found to be qualitatively consistent with the predictions based on the classical colloidal stability theory. The presence of low levels (1−6 mg/L) of Suwannee River humic acid, fulvic acid, alginate, citric acid, and carboxymethyl cellulose greatly enhanced the stability and mobility of CeO_2 NPs in 1 mM NaCl at pH 6.5. The poor correlation between the transport behavior and electrophoretic mobility of CeO_2 NPs implies that the electrosteric effect of OM was involved.

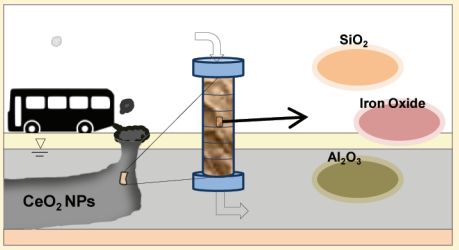

INTRODUCTION

Many nanotechnology breakthroughs have begun to impact the marketplace. The nanotechnology products are estimated to achieve a $3 trillion market with six million workers by 2020. [1] Potential risks of the exposure to nanomaterials, however, have become a major concern when released to the environment. Cerium dioxide (CeO_2) is among the priority list of manufactured nanomaterials for evaluation, based on materials in, or close to, commerce. [2] The CeO_2 nanoparticles (NPs) have gained a wide range of applications in daily life products, catalysts, and therapy. One example is the application in diesel additive to reduce NO_x and particulate emissions, however, the level of CeO_2 increases significantly in the ambient air.[3,4] The CeO_2 NPs in the atmosphere will deposit on environmental surfaces and enter water, soil, and subsurface ultimately. When interacting with fauna, CeO_2 NPs show toxicity in aquatic environments toward bacteria, algae, and even human cells.[5−8]

The bioavailability and potential nanotoxicity is greatly influenced by the stability and transport behavior of NPs in the environment. NPs aggregate fast and settle out of the liquid phase when the ionic strength is larger than a critical coagulation concentration (CCC). For instance, the CCC for CeO_2 NPs was reported to be 34 and 80 mM at pH 5.6 and 11.0, respectively, in monovalent electrolytes (KCl or NaCl).[9,10] When entering the wastewater plant, a significant fraction of the CeO_2 NPs can escape the treatment system, although the majority could be captured by the sludge. [11] Partial breakthrough of CeO_2 NPs was observed at neutral to alkaline pH and ionic strength below 10 mM, and NPs can be detached from porous media by changing the solution chemistry. [12] The presence of natural organic matter (NOM) increases the absolute value of ζ-potential of the coated CeO_2 NPs, and prevents the NPs from directly interacting with each other and with algal cells.[13,14] Furthermore, the retention of CeO_2 on soils was proposed to be associated with naturally occurring colloids, such as Al, Si, and Fe oxides. [15] However, investigations to quantify the influence of soil composition and organic matter (OM) on the transport of CeO_2 NPs have not been reported in the literature.

In this study, we comprehensively studied the deposition behavior of CeO_2 NPs in dilute NaCl solutions using two approaches, i.e. quartz crystal microbalance with dissipation (QCM-D) and column experiments. Since iron oxide and alumina (Al_2O_3) patches on mineral grains are suggested to predominantly influence the colloid transport in subsurface

Received: March 5, 2012
Revised: May 18, 2012
Accepted: May 23, 2012
Published: May 23, 2012

environment, [16] the iron oxide, Al_2O_3 and silica (SiO_2) coated sensors were applied to quantify the effect of the soil mineral components on the deposition kinetics of CeO_2 NPs using QCM-D. The flow geometry in the QCM-D chamber is similar to parallel plate flow, which is not always representative of the natural environment, and therefore, column experiments were conducted to simulate the hydraulic conditions with better environmental relevance as a supplement to the QCM-D study. Traditional Derjaguin–Landau–Verwey–Overbeek (DLVO) calculations were conducted, and the non-DLVO forces were discussed to interpret and reconcile the seemingly conflicting data obtained from the two experimental approaches. This study aims to evaluate the key environmental factors that dominantly influence the stability and transport of CeO_2 NPs in aquatic environments.

MATERIALS AND METHODS

Preparation of CeO_2 NP Dispersions. A 25-mg portion of CeO_2 NPs (Strem Chemicals Inc., Newburyport, MA) was dispersed in 0.5 L of DI water in Teflon bottles and ultrasonicated for 1 h in an ultrasonic bath (Branson 1510, 40 kHz, 120 V). Background ionic strength (e.g., 10 mM) was adjusted with addition of a stock solution of 5 M NaCl, and the pH was adjusted using HCl and NaOH stock solutions after ultrasonication. Leaving the dispersion quiescent for 1 h, the main part of CeO_2 dispersion was separated carefully from the aggregates that settled out of the aqueous phase. The preparation protocol for NP suspension has been used in studies on the fate and transport of commercial nanomaterials in the literature.[17−19] For experiments in the presence of OM, CeO_2 dispersions were amended with various OM to final concentrations of 1−6 mg/L. After ultrasonication and settling for 24 h, the main part of dispersion was separated from aggregates out of the liquid phase, so that similar CeO_2 concentration was obtained compared with that in the absence of OM (Table S1, SI). The tested OM included Suwannee River humic acid (SRHA, International Humic Substances Society), Suwannee River fulvic acid (SRFA, International Humic Substances Society), citric acid (CA, J.T. Baker, Phillipsburg, NJ), alginic acid sodium salt (from brown algae, Sigma-Aldrich), and sodium carboxymethyl cellulose (CMC, Sigma-Aldrich, St. Louis, MO).

Characterization of CeO_2 NPs. The hydrodynamic diameter of the suspended CeO_2 NPs was obtained on a Zetasizer (Nano ZS, ZEN3600, Malvern, U.K.) using dynamic light scattering (DLS). Details on DLS instrument and experimental procedure can be found in an early study. [20] Electrophoretic mobility (EPM) was measured, and the ζ-potential was obtained using the Henry Equation. [21] The point of zero charge (PZC, the pH when EPM = 0) was determined by means of EPM measurement in 10 mM NaCl at varying pH values. All DLS measurements were conducted, at a minimum, in duplicates at 25 °C.

Transmission electron microscopy (Philips FEI CM20 FEG S/TEM) was used to examine the morphology of CeO_2 NPs, as described earlier. [20] The crystallinity of the CeO_2 NPs was assessed using an X-ray diffractometer (Rigaku Miniflex) (SI). Scanning electron microscopy with energy-dispersive X-ray spectroscopy (SEM-EDS) (JEOL-6360 with EDS/OXFORD INCA software) was used to estimate the chemical compositions of CeO_2 NPs and QCM-D sensors. To estimate the amounts of impurities in CeO_2 and silica sand, microwave-assisted HNO_3-digestion and hot plate acid digestion methods were used followed by elemental determination by Inductively Coupled Plasma–Optical Emission Spectroscopy (ICP −OES) and ICP–Mass Spectrometry (ICP–MS). [20]

QCM-D Experiment. The experiments of CeO_2 deposition were conducted in the Q-sense E1 system (Västra Frölunda, Sweden) to examine the influence of collector surface composition, pH, and electrolyte (NaCl) concentration. SiO_2 (QSX 303), Al_2O_3 (QSX 309), and iron oxide (QSX 236) coated quartz crystal sensors (5 M Hz) were cleaned before use according to the recommended protocols. Briefly, SiO_2 sensors were treated by UV/ozone (ProCleaner, Bioforce Nanosciences, Ames, IA) for 15 min and then immersed in 2% sodium dodecyl sulfate (SDS) solution for 30 min. Al_2O_3 and iron oxide sensors were sonicated in ethanol. The sensors were rinsed with DI water and dried with nitrogen gas. The flow rate was 0.100 ± 0.001 mL/min for all experiments and temperature was set at 22 °C. Background solution with the desired pH and ionic strength (1−200 mM) was introduced to equilibrate the QCM-D sensor surface before experiment. The system was considered to be stabilized when the normalized third overtone frequency shift (Δf_3) was less than 0.3 Hz in 10 min. [22] When NPs deposited onto crystal sensors, the mass change (Δm) of the crystal induced a shift in the overtone frequency (Δf_n) as described by the Sauerbrey relationship (SI).[23−25] Both f and dissipation (D) at the third overtone was used to quantify the deposition kinetics of CeO_2 NPs at early stage (~15−60 min). The ζ-potential of the SiO_2 coated sensors was estimated by measurement of quartz colloids using the method in the literature. [26]

Column Experiment. Glass columns (Kontes, Vineland, NJ) with a length of 15 cm and inner diameter of 2.5 cm were used. The Ottawa sand (U.S. Silica, Berkeley Spring, WV) was sifted through 250−300 μm sieves (50−60 mesh size, ATM, New Berlin, WI) and cleaned thoroughly using concentrated HCl. [27] An average quantity of 129.6 g of sand was packed into each cylindrical column by wet method, yielding an approximate porosity of 0.387. A nylon spectra filter with a pore size of 70 μm was put at the bottom of the column to support the sand media. Approximately 24 pore volumes (PV, 28.46 mL) of background solutions (10 mM NaCl adjusted separately to pH 4.0, 6.0, and 8.5 to test the effect of pH, and 1 mM or 20 mM NaCl (one test) at pH 6.5 to test the effect of OM) were preintroduced into each column using two syringe pumps (100 mL, Harvard Apparatus, Holliston, MA) to allow chemical equilibration with background solutions. [28] The first 12 PV of background solution was introduced upward to exclude entrapped air bubbles, followed by another 12 PV of background solution introduced downward to be consistent with environmental subsurface scenario.

CeO_2 NP dispersions were introduced downward into saturated sand at a flow rate of 1.5 mL/min (approaching fluid velocity of 1.32×10^{-4} m/s). The column experiment procedure was separated to 3 steps: 6 PV of CeO_2 NP dispersions (step I), 2 PV of NP-free background solutions (step II), and 4 PV of DI water (step III). An automatic collector was used to collect effluent samples and CeO_2 concentration was measured using ICP-OES after microwave-assisted HNO_3 digestion. [20] ICP-MS was also used if the measurement was lower than the detection limit of ICP-OES, i.e., 0.011 mg/L for aqueous samples or 0.400 mg/kg for solid (sand) samples.

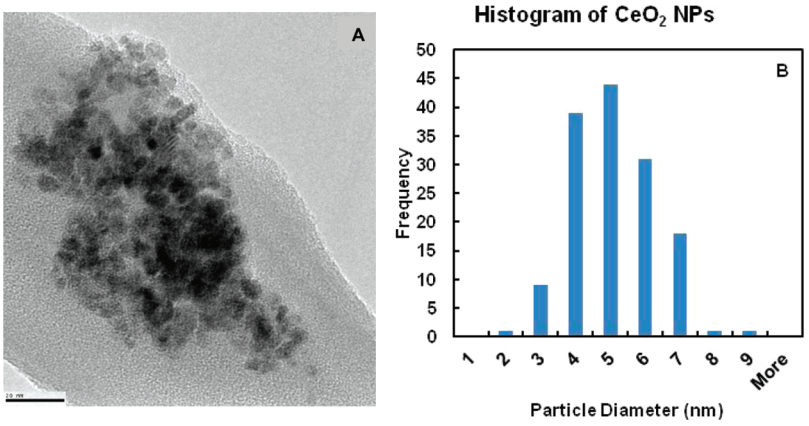

Figure 1. (A) Transmission Electron Microscopy (TEM) image of CeO_2 NPs with the scale bar equal to 20 nm; (B) particle size distribution of CeO_2 NPs based on the measurement of 144 particles using TEM and ImageJ software.

RESULTS AND DISCUSSION

Characterization of CeO_2 NPs. The CeO_2 NPs were mainly spherical particles with a slight angular appearance as shown in the TEM image (Figure 1A). The average diameter was obtained to be 4.6 nm, and 79.2% of NPs ranged from 3 to 5 nm in measurement of 144 particles using ImageJ software (National Institutes of Health) (Figure 1B). The hydrodynamic diameter was 172 nm, as obtained by DLS at the unadjusted pH (4.6) in DI water. The signal of scattered light deviated toward larger aggregates, leading to much larger hydrodynamic size compared with the individual NP size in TEM image. The major elements were cerium and oxygen as indicated by SEM-EDX spectra (Figure S1-A of the SI). ICP-OES/MS data revealed a small amount of impurities in the NPs, such as Na (0.04%), Ca (0.02%), Pb (0.02%), Al (0.01%), etc. (hot plate digestion applied, Table S3 of the SI). The CeO_2 NPs were crystalline rather than amorphous as revealed by the XRD pattern (Figure S1-B of the SI), which had the same *d*-spacing values as in the literature (SI). The unadjusted pH of CeO_2 dispersion was 4.6 ± 0.2 after sonication, close to the reported value of 4.5 in the literature. [15] The CeO_2 NPs were positively charged at pH 4.6 in DI, with an EPM value of 1.266 μm·cm/(V·s).

Influence of pH on the Stability of CeO_2 NPs. EPM and particle size were monitored at various pH values in 10 mM NaCl or 1 mM $CaCl_2$ solutions. The measurement was conducted at different times, i.e., after the pH value was immediately adjusted or equilibrated overnight. Figure 2 revealed that the EPM data measured immediately were similar to that after overnight equilibration at 10 mM NaCl. The CeO_2 NPs became less positively charged with the increase in pH from 2.5 to 6.8. With further increase in pH from 6.8 to 11.5, the CeO_2 NPs became more negatively charged. The EPM of CeO_2 at 1 mM $CaCl_2$ was consistent with that at 10 mM NaCl within acidic to neutral pH range. However, at pH ≥ 9.1, the EPM at 1 mM $CaCl_2$ was less negative than that at 10 mM NaCl. The CeO_2 NPs became less negatively charged with further increase in pH to pH 11.5 at 1 mM $CaCl_2$. The less negative charge at 1 mM $CaCl_2$ could possibly be attributed to the complexation of OH^- groups with the Ca^{2+} ions to form $Ca(OH)^+$ on the NP surface under basic conditions. A similar trend line was also found for the ζ-potential of titanium dioxide (TiO_2) NPs at 1 mM $CaCl_2$ at pH 8 − 9. [29] In summary, the PZC for CeO_2 NPs was determined to be approximately pH 6.8. This value falls within the reported PZC range of 3.0−7.6 for CeO_2 in the literature.[9,10,12] Such a wide range of PZC could be attributed to NP impurities introduced in the NP synthesis processes,[9,30] which largely determine the surface properties and stability of engineered NPs in the aqueous phase. [20]

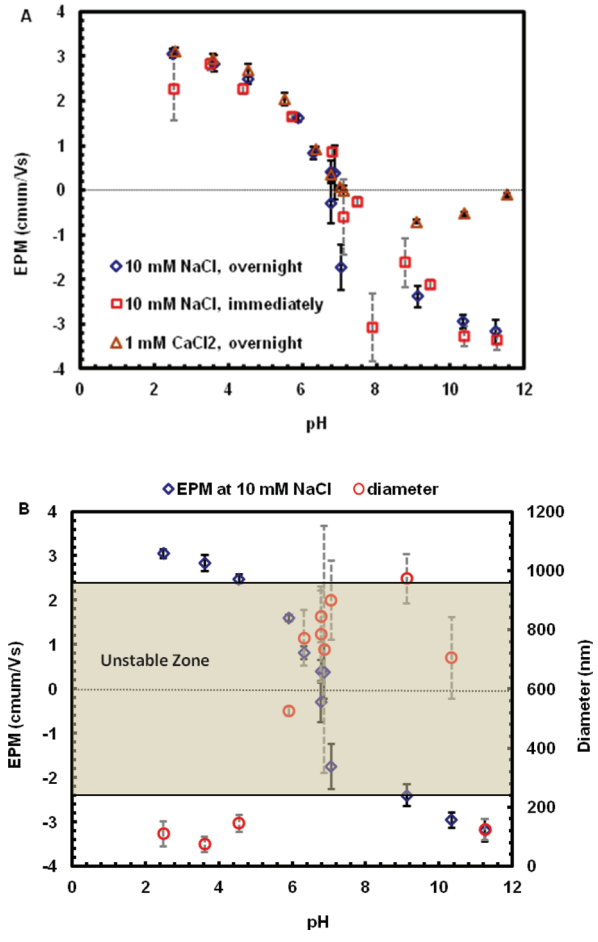

Figure 2. (A) Electrophoretic mobility (EPM) of CeO_2 NPs in10 mM NaCl or 1 mM $CaCl_2$ measured immediately and after overnight equilibration; (B) EPM and hydrodynamic diameter of CeO_2 NPs in 10 mM NaCl after overnight equilibration as a function of pH. The error bars represent the sample standard deviations, obtained from at least three replicate measurements.

dx.doi.org/10.1021/es300883q | Environ. Sci. Technol. 2012, 46, 6681−6688

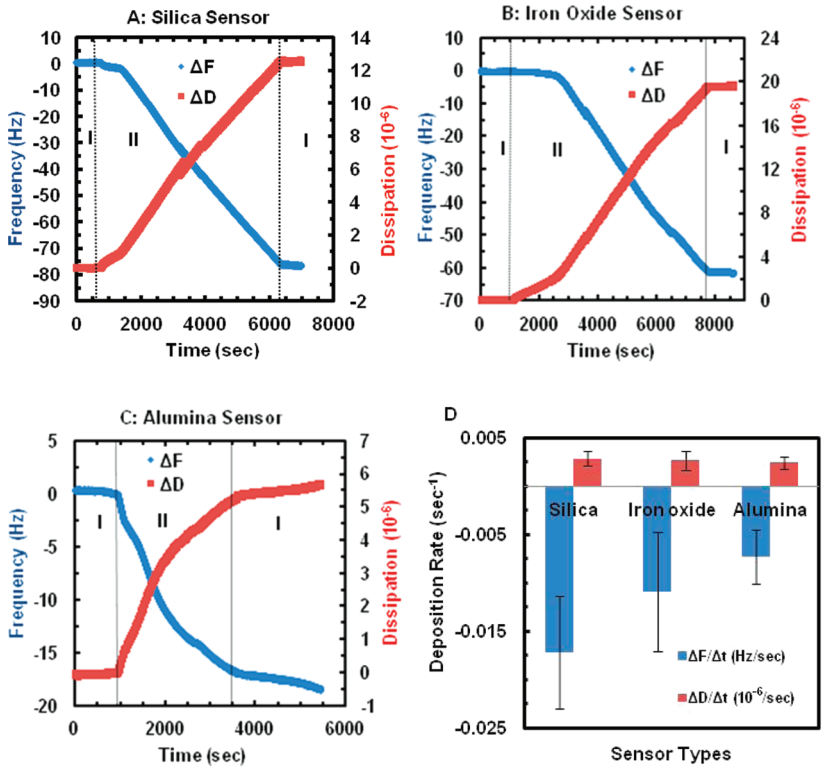

Figure 3. Representative frequency and dissipation shifts (from the third overtone measurements) for the deposition of CeO_2 NPs on (A) SiO_2, (B) iron oxide, and (C) Al_2O_3 coated crystal sensors at pH 4.0. (D) The average frequency and dissipation shift rates for the deposition of CeO_2 NPs on the various surfaces with error bars representing the sample standard deviations obtained from at least three replicate measurements.

The hydrodynamic size shows a generally consistent trend with the EPM measurement. The hydrodynamic size increased from pH 2.5 (111 nm) to pH 9.1 (974 nm), and then decreased with further increase in pH (Figure 2B). Within the pH range of 4.5−9.1, the decreased value of EPM resulted in less electrostatic repulsion and aggregation between CeO_2 NPs. Nevertheless, at pH < 4.5 or pH > 9.1, the absolute value of EPM was larger than 2.4 μm·cm/V·s. It appears that the electrostatic repulsion was sufficient to stabilize CeO_2 NPs, which was indicated by the measured minimum value of the hydrodynamic size of ∼110 nm. A critical EPM range of −2 to −0.8 μm·cm/V·s was reported for TiO_2, zinc oxide (ZnO), and CeO_2 NPs, where the transition from reaction to diffusion limited aggregation occurs. [31] As expected, the stability of CeO_2 NPs in aqueous suspensions was related to their EPM values.

Effect of Collector Surface Composition and pH on the Deposition of CeO_2 NPs: QCM-D Experiments. SiO_2 sensors were applied in QCM-D because it is the major chemical composition of sand. The linear decrease of frequency was observed at pH 4.0 (Figure 3A), when background solution (step I) was switched to CeO_2 suspension (step II) at 10 mM NaCl. Meanwhile, the dissipation was found to increase linearly with increasing time. This indicates the deposition of CeO_2 NPs on SiO_2 surface. In contrast, no significant deposition of CeO_2 was observed on SiO_2 sensors at pH 6.0 or pH 8.5 (Figure S2 of the SI). We conducted interaction energy calculations, using the equation for van der Waals attraction proposed by Gregory considering retardation,[32] and electrostatic interaction based on the linear superposition approximation. [33] The Hamaker constant was taken as 9.07×10^{-21} J for the CeO_2−H_2O−SiO_2 system (as calculated in the SI). Figure S3 of the SI revealed that the attractive interaction extends to a distance of >10 nm, when a CeO_2 NP approaches SiO_2 surface at pH 4.0. Similarly, Pomorska et al. reported the deposition of TiO_2 on SAM modified Au surfaces with opposite charges in QCM experiments. [34] The energy profile at 6.5 is similar to that at pH 4.0. At pH 8.5, nevertheless, the energy barrier was 20 kT. The magnitude of the barrier is sufficient to prevent most CeO_2 NPs from approaching SiO_2 surface by Brownian motion, because the average Brownian kinetic energy is on the order of 1 kT. [35] Similar to this study, no deposition was found for TiO_2 NPs on SiO_2 sensors at pH ≥ 8 in QCM-D experiments.[25,29] The deposition of CeO_2 NPs was in accordance with the predictions based on the DLVO calculation at pH 4.0 and 8.5. However, the QCM-D data at pH 6.0 was not consistent with theoretical predictions. This deviation is discussed in detail in the following sections.

Iron oxide and Al_2O_3 coated sensors were applied to investigate the influence of the collector surface composition as an indicator of chemical heterogeneity on the deposition of CeO_2 NPs. Significant deposition was observed on both iron oxide and Al_2O_3 surfaces at pH 4.0 (Figure 3B,C). The frequency shift rates, $d\Delta f/dt$, for the deposition of CeO_2 on iron oxide (−0.0109 Hz/sec) and Al_2O_3 surfaces (−0.0073 Hz/sec) were smaller than that on SiO_2 surface (−0.0172 Hz/sec) at pH 4.0. The same trend was observed for the rates of dissipation shift, $d\Delta D/dt$ (Figure 3D). This could be attributed to the fact that SiO_2 was probably more negatively charged than iron oxide and Al_2O_3 surfaces. To reveal the surface nature, we characterized the composition and crystallinity of the crystal sensors using EDX and XRD (Figures S4 and S5, SI). The expected elements, such as Si, Fe, Al, and O, were verified by EDX. However, the XRD signals of iron oxide and Al_2O_3 were overwhelmed by the gold electrode and quartz crystal

dx.doi.org/10.1021/es300883q | Environ. Sci. Technol. 2012, 46, 6681−6688

underneath (Figure S4, SI). The iron oxide coated sensor is advertised as Fe_3O_4, which is, however, easily oxidized in aerated water to form maghemite. In the analysis using X-ray photoelectron spectroscopy, published Fe 2p 3/2 binding energies show a significant overlap for Fe_2O_3, Fe_3O_4, and FeOOH. [36] Hence, it deserves further investigation to understand what specific mineral phases in natural sediments might be represented by these sensors. In a recent study, Lin et al. reported the favorable deposition of silver NPs on the hematite coated sands. [37] It is noticed that the role of iron oxide and Al_2O_3 is more significant on the deposition of NPs under unfavorable conditions.

Column Experiments. The concentration of CeO_2 NPs in the effluent generally increased for the first 2 PV, and then reached a relatively stable plateau (Figure 4A). The normalized concentration (C/C_0) at plateau was 0.4%, 1%, and 4.3%, respectively, at pH 4.0, 6.0, and 8.5. Such a low effluent concentration at pH 8.5 is not consistent with the DLVO prediction, which could be attributed to the non-DLVO interactions as discussed later. The effluent concentration decreased with no tailing when NP-free background solution was introduced (step II). A small amount of NP re-entrainment was observed at pH 8.5 when rinsed by DI water at step III (Figure 4A). Li et al. observed similar effluent data at step I and much higher re-entrainment concentration at step III at pH 6 and 9 for CeO_2 NPs with larger size (5−60 nm) and heterogeneous morphology. [12] The CeO_2 NPs in their study were more negatively charged at the same pH and ionic strength, and therefore the influence of secondary minimum is more remarkable than that in this study.

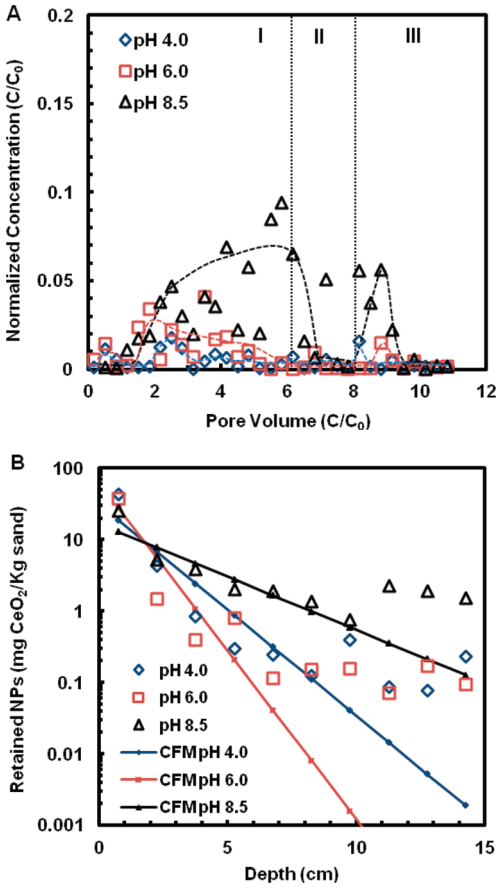

Figure 4. (A) Breakthrough curves and (B) retention profiles for CeO_2 NPs in 10 mM NaCl at pH 4.0, 6.0, and 8.5 in column experiment. Dashed lines in A were drawn as a guide to the eye, solid lines in B were derived from equations of the classical filtration model (CFM).

The retention of CeO_2 on sand was 99.2%, 97.9%, and 94.3% of the totally introduced amount at pH 4.0, 6.0, and 8.5, respectively. Most CeO_2 NPs deposited at the first 1 cm of sand from the inlet (Figure 4B). At pH 4.0 and 8.5, the amount of retained CeO_2 decreased exponentially along column to the depth of ~9.75 cm, which generally followed the classical filtration model (CFM) curve. Since the repulsive interaction was not dominant, such consistent fitting with the CFM could be expected. [26] Deviation from CFM was observed with further increase in the column depth from 9.75 cm to the end at pH 4.0 and 8.5, which might be attributed to the redistribution of NPs during rinsing process. [12] The CFM fitting was not good at pH 6.0. This could be attributed to the tested pH (6.0) near the PZC of the CeO_2 NPs (pH 6.8). The aggregation at pH 6.0 resulted in a wide distribution of NP size, leading to higher drag force, and the difficulty in the estimation of fitting parameters, such as single collector efficiency, η.

Deviation of QCM-D from Column Experiments: Influence of NP Aggregation, Flow Geometry, and Surface Heterogeneity. Contrary to at pH 4.0, no noticeable deposition was observed at pH 6.0 and 8.5 on any type of the tested sensors in QCM-D experiments (Figure S2, SI). The profiles of DLVO interaction energy reveal that attraction is dominant between positively charged CeO_2 NPs and negatively charged SiO_2 surface at pH 6.0 (Figure S3-A, SI). The deviation of QCM-D data could be attributed to the aggregation of CeO_2 NPs at pH 6.0 (Figure 2B). The aggregation of NPs resulted in weaker convective-diffusive transport due to the increased size, and also less probability of collision to sensor surface because of the decreased NP/aggregate number. [25] Moreover, a particle/aggregate with larger diameter experiences an increased hydrodynamic drag force near a planar wall in a shear linear flow. [38] The drag force for large aggregates could increase to the magnitude that is sufficient to influence the detachment and deposition (SI). Nevertheless, due to the complex flow geometry in a column, the irregular shape and surface roughness of Ottawa sand lead to low velocity regions,[39] where net force (sum of the DLVO and fluid drag force) could be zero in the rear stagnation point within sand grains. [40] In addition, straining may affect the deposition of CeO_2 NPs in sand media when concurrent NP aggregation happens at pH 6.0. At pH 8.5, the DLVO calculation reveals that CeO_2 NPs could not break through the energy barrier (20 kT) to contact the SiO_2 surface (Figure S3-A, SI), which is in accordance with QCM-D data. In column test, nevertheless, the value for C/C_0 was only 4.4% and 94.3% of introduced CeO_2 NPs were retained on the surface of sand. Again, the retained CeO_2 NPs under the unfavorable condition could be attributed to the physical (roughness) and chemical heterogeneity of the sand surface that served as favorable sites for the attachment.[40,41] Metallic elements such as Fe and Al, were found on the Ottawa sand surface even after careful washing by concentrated HCl (Table S6, SI). The heterogeneity may also arise from the impurities within mineral matrices that are exposed on the surface after removal of surface coating. [42] The magnitude for both van de Waals and electrostatic interactions decreases for NPs approaching a surface with roughness, which tends to render the surface more attractive.[43,44] Other properties of

dx.doi.org/10.1021/es300883q | Environ. Sci. Technol. 2012, 46, 6681−6688

surface heterogeneities, such as composition and crystallinity, require further investigation to clarify the influence on the interaction of NPs with environmental media.

Deposition Kinetics of CeO_2 NPs: Effect of Ionic Strength. Deposition kinetics was conducted at the unadjusted pH value of 4.6 using QCM-D. The attachment efficiency, α, can be defined as follows:[45]

$$\alpha_F = \frac{\frac{d\Delta f_{(3)}}{dt}}{\left(\frac{d\Delta f_{(3)}}{dt}\right)_{diff}} \quad (1)$$

$$\alpha_D = \frac{\frac{d\Delta D_{(3)}}{dt}}{\left(\frac{d\Delta D_{(3)}}{dt}\right)_{diff}} \quad (2)$$

In eqs 1 and 2, the frequency or dissipation shift was normalized by that in the diffusion controlled regime. At the lowest NaCl concentration (2 mM), the maximum value of α_F was obtained as 16.9 for frequency shift (Figure 5A). As shown in Figure S6 (SI), the attractive interaction energy extended to a longer distance and enhanced the transport of NPs toward crystal sensors. [46] The α_F decreased with the increase of NaCl concentrations from 2 to 10 mM. The increased concentrations of NaCl compressed the thickness of electric double layer (EDL) and the absolute values of surface potential decreased for both CeO_2 NPs and SiO_2 surface (Figure 5B). As a result, deposition rates decreased with the decrease in the magnitude and range of attractive EDL attraction. The α_F value was close to unity at 10 mM NaCl and did not change greatly with further increase in NaCl concentrations. The critical deposition concentration (CDC) was determined to be 10 mM NaCl. When NaCl concentrations are higher than CDC, the range of the EDL attraction is not sufficiently large to enhance the transport of NPs toward the collector surface, and deposition rates are controlled by van der Waals and hydrodynamic interactions. [47] The attachment efficiency curves were consistent with each other for the monitoring of dissipation and frequency shift. The CDC was close to the reported value by Li et al. in column study at pH 6. [12] Compared with other QCM-D studies, the CDC for CeO_2 was smaller than TiO_2 and ZnO NPs on bare SiO_2 sensors. For instance, the CDC was 60 mM $NaNO_3$ for 5 nm TiO_2 at pH 3,[25] ~100 mM NaCl for 30 nm TiO_2 at pH 5−7 [29] and 150 mM NaCl for ZnO NPs at pH 7.8. [48] This indicates that CeO_2 may be less mobile than TiO_2 and ZnO in the absence of OM at similar ionic strength within the weakly acidic to neutral pH range.

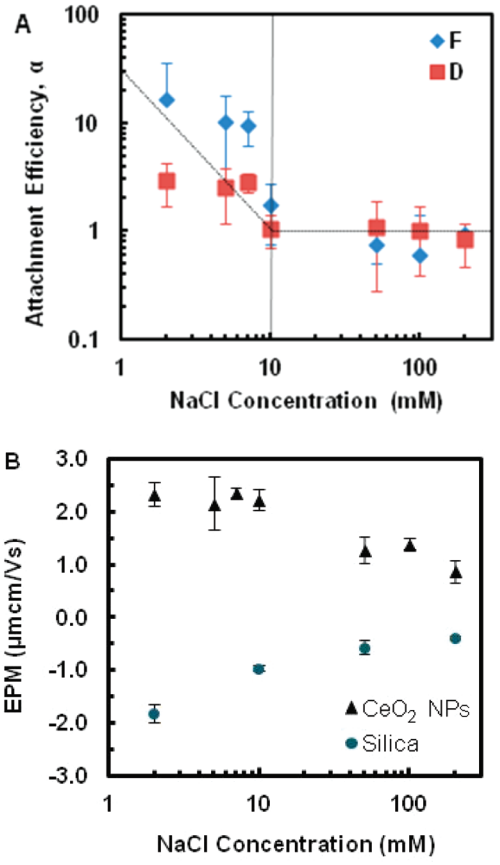

Figure 5. Attachment efficiency for the deposition of CeO_2 NPs on SiO_2 sensors based on the third overtone frequency shift, Δf, and dissipation shift, ΔD, as a function of NaCl concentration at the unadjusted pH (4.6) in QCM-D experiment; (B) The EPM of CeO_2 NPs and SiO_2 colloids under the QCM-D experimental conditions. The error bars represent the sample standard deviations obtained from at least two replicate measurements.

Influence of Organic Matter on the Deposition of CeO_2 NPs. The presence of OM greatly enhanced the transport of CeO_2 NPs at neutral pH (Figure 6A). The steady normalized concentrations (C/C_0) were ≥0.782 in the effluent of column experiments at 1−6 mg/L OM, compared with that of 0.012 in the absence of OM. The EPM of CeO_2 in the presence of tested OM was about 3 times higher than that in the absence of OM (Table S1, SI). For the effect of OM concentration, the normalized values of C/C_0 at plateau were close in the presence of 3 and 6 mg/L SRHA, i.e., ~1.0 and 0.932, respectively. Both values are higher than that in the presence of 1 mg/L SRHA (0.782). Nevertheless, the EPM for CeO_2 in the presence of 1 mg/L SRHA, i.e., −3.743 μm·cm/V·s, was close to that in 6 mg/L SRHA (−3.867 μm·cm/V·s). Therefore, the higher CeO_2 concentrations in the effluent might be due to higher adsorption of SRHA on both Ottawa sand and NPs at 3 and 6 mg/L SRHA, conditions under which steric effects plays an influential role. In addition, when relating the EPM to the transport data, combined steric with electrostatic (electrosteric) effect could also be implied. If the electrostatic interaction was the only dominant factor, then the CeO_2 concentration in the effluent should increase with the absolute value of EPM, which was not observed in Figure 6B. Similarly, the electrosteric interaction was also found to be dominant for NP−NP interaction in the presence of OM. For instance, Deonarine et al. recently reported the inconsistency between ζ-potential and growth rates of ZnS NPs, and attributed it to the additional steric interactions in the presence of OM. [49]

■ ENVIRONMENTAL IMPLICATIONS

Water chemistry (pH, ionic strength, and organic matter) was observed to influence the stability of CeO_2 NPs in aqueous environment. The CeO_2 NPs aggregate and tend to settle out of the liquid phase at neutral pH close to the PZC of 6.8. Iron oxide is an important component of the chemical heterogeneity of the collector surface for the deposition of CeO_2 NPs, with a higher deposition rate than the Al_2O_3 surface at pH 4.0 in QCM-D experiments. No significant deposition of the CeO_2 was observed at pH 6.0 or 8.5 on any of the tested surfaces in

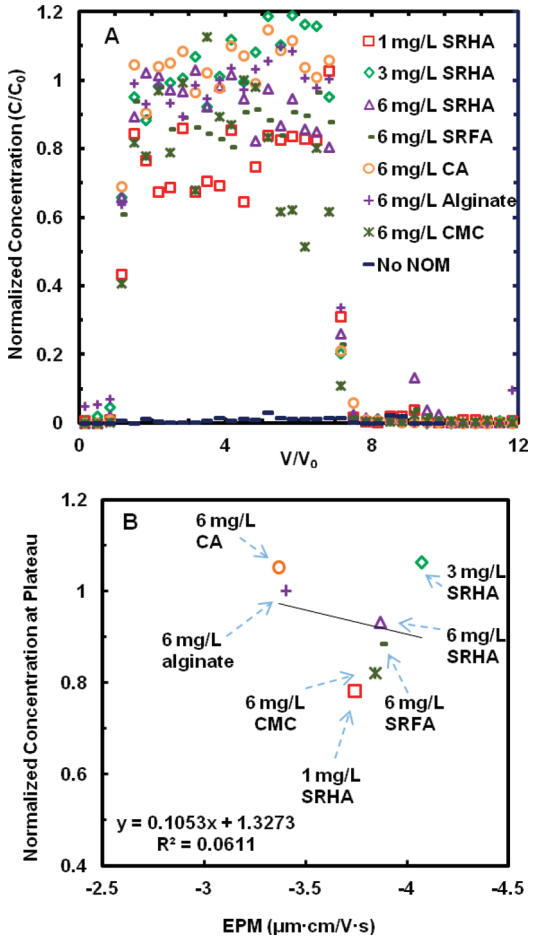

Figure 6. (A) Breakthrough curves for the transport of CeO_2 NPs in the presence of various OM; (B) correlation of the normalized concentrations, C/C_0, with the EPM of CeO_2 NPs in the presence of various OM in column experiments.

QCM-D experiment, due to the aggregation of NPs and repulsion between NPs and surfaces, respectively. In contrast, most of the NPs deposited on the surface of Ottawa sand in column experiments at pH 6.0 and 8.5, which could be mainly attributed to the surface roughness, chemical patchwise heterogeneities, and low velocity regions within sand media. The stability and mobility of CeO_2 NPs was greatly enhanced in the presence of SRHA, SRFA, citric acid, alginate, and CMC due to electrosteric effect. Further study is needed to investigate detailed mechanisms of this enhancement. This may include determining quantities of OM adsorption on NPs and sand grains as influenced by different functional groups in OM and the interactions with divalent cations. By doing so, a more complete understanding of the transport of CeO_2 NPs in natural environment can be achieved.

■ ASSOCIATED CONTENT

Supporting Information

Six additional figures, nine tables, and text are available. This information is available free of charge via the Internet at http://pubs.acs.org/.

■ AUTHOR INFORMATION

Corresponding Author

*Phone: (580) 436-8803 (X.L.), (580) 436-8638 (C.S.); fax: (580) 436-8703 (C.S.); e-mail: liu.xuyang@epa.gov (X.L.), su.chunming@epa.gov (C.S.).

Notes

The authors declare no competing financial interest.

■ ACKNOWLEDGMENTS

This study was funded by the National Nanotechnology Initiative through the U.S. Environmental Protection Agency (U.S. EPA). It has not been subjected to the Agency's peer and administrative review, and therefore, does not necessarily reflect the views of the Agency, and no official endorsement should be inferred.

■ REFERENCES

(1) Roco, M. C.; Mirkin, C. A.; Hersam, M. C. *Nanotechnology Research Directions for Societal Needs in 2020: Retrospective and Outlook*; Springer: New York, 2011.

(2) *Nanosafety at the OECD: The First Five Years 2006–2010*; Organization for Economic Cooperation and Development: Paris, France, 2011; http://www.oecd.org/dataoecd/6/25/47104296.pdf.

(3) *Evaluation of Human Health Risk from Cerium Added to Diesel Fuel*; Health Effects Institute: Boston, MA, 2001; http://pubs.healtheffects.org/getfile.php?u=295.

(4) *Nanotechnology White Paper*; EPA 100/B-07/001; U.S. Environmental Protection Agency: Washington, DC, 2007; http://www.epa.gov/osa/pdfs/nanotech/epa-nanotechnology-whitepaper-0207.pdf.

(5) Zhang, H.; He, X.; Zhang, Z.; Zhang, P.; Li, Y.; Ma, Y.; Kuang, Y.; Zhao, Y.; Chai, Z. Nano-CeO_2 exhibits adverse effects at environmental relevant concentrations. *Environ. Sci. Technol.* **2011**, *45* (8), 3725–3730.

(6) Thill, A.; Zeyons, O.; Spalla, O.; Chauvat, F.; Rose, J.; Auffan, M.; Flank, A. M. Cytotoxicity of CeO_2 nanoparticles for *Escherichia coli*. Physico-chemical insight of the cytotoxicity mechanism. *Environ. Sci. Technol.* **2006**, *40* (19), 6151–6156.

(7) Van Hoecke, K.; Quik, J. T. K.; Mankiewicz-Boczek, J.; De Schamphelaere, K. A. C.; Elsaesser, A.; Van Der Meeren, P.; Barnes, C.; McKerr, G.; Howard, C. V.; Van De Meent, D.; Rydzyński, K.; Dawson, K. A.; Salvati, A.; Lesniak, A.; Lynch, I.; Silversmit, G.; De Samber, B.; Vincze, L.; Janssen, C. R. Fate and effects of CeO_2 nanoparticles in aquatic ecotoxicity tests. *Environ. Sci. Technol.* **2009**, *43* (12), 4537–4546.

(8) Rogers, N. J.; Franklin, N. M.; Apte, S. C.; Batley, G. E.; Angel, B. M.; Lead, J. R.; Baalousha, M. Physico-chemical behaviour and algal toxicity of nanoparticulate CeO_2 in freshwater. *Environ. Chem.* **2010**, *7* (1), 50–60.

(9) Buettner, K. M.; Rinciog, C. I.; Mylon, S. E. Aggregation kinetics of cerium oxide nanoparticles in monovalent and divalent electrolytes. *Colloids Surf., A* **2010**, *366* (1–3), 74–79.

(10) Li, K.; Zhang, W.; Huang, Y.; Chen, Y. Aggregation kinetics of CeO_2 nanoparticles in KCl and $CaCl_2$ solutions: Measurements and modeling. *J. Nanopart. Res.* **2011**, 1–9.

(11) Limbach, L. K.; Bereiter, R.; Muller, E.; Krebs, R.; Galli, R.; Stark, W. J. Removal of oxide nanoparticles in a model wastewater treatment plant: Influence of agglomeration and surfactants on clearing efficiency. *Environ. Sci. Technol.* **2008**, *42* (15), 5828–5833.

(12) Li, Z.; Sahle-Demessie, E.; Hassan, A. A.; Sorial, G. A. Transport and deposition of CeO_2 nanoparticles in water-saturated porous media. *Water Res.* **2011**, *45* (15), 4409–4418.

(13) Quik, J. T. K.; Lynch, I.; Hoecke, K. V.; Miermans, C. J. H.; Schamphelaere, K. A. C. D.; Janssen, C. R.; Dawson, K. A.; Stuart, M. A. C.; Meent, D. V. D. Effect of natural organic matter on cerium dioxide nanoparticles settling in model fresh water. *Chemosphere* **2010**, *81* (6), 711–715.

(14) Van Hoecke, K.; De Schamphelaere, K. A. C.; Van der Meeren, P.; Smagghe, G.; Janssen, C. R. Aggregation and ecotoxicity of CeO_2 nanoparticles in synthetic and natural waters with variable pH, organic matter concentration and ionic strength. *Environ. Pollut.* **2011**, *159* (4), 970−976.
(15) Cornelis, G.; Ryan, B.; McLaughlin, M. J.; Kirby, J. K.; Beak, D.; Chittleborough, D. Solubility and batch retention of CeO_2 nanoparticles in soils. *Environ. Sci. Technol.* **2011**, *45* (7), 2777−2782.
(16) Elimelech, M.; Nagai, M.; Ko, C. H.; Ryan, J. N. Relative insignificance of mineral grain zeta potential to colloid transport in geochemically heterogeneous porous media. *Environ. Sci. Technol.* **2000**, *34* (11), 2143−2148.
(17) Saleh, N. B.; Pfefferle, L. D.; Elimelech, M. Aggregation kinetics of multiwalled carbon nanotubes in aquatic systems: Measurements and environmental implications. *Environ. Sci. Technol.* **2008**, *42* (21), 7963−7969.
(18) Ghosh, S.; Mashayekhi, H.; Pan, B.; Bhowmik, P.; Xing, B. Colloidal behavior of aluminum oxide nanoparticles as affected by pH and natural organic matter. *Langmuir* **2008**, *24* (21), 12385−12391.
(19) Liu, X.; Wazne, M.; Chou, T.; Xiao, R.; Xu, S. Influence of Ca^{2+} and Suwannee River Humic Acid on aggregation of silicon nanoparticles in aqueous media. *Water Res.* **2011**, *45* (1), 105−112.
(20) Liu, X.; Chen, G.; Su, C. Effects of material properties on sedimentation and aggregation of titanium dioxide nanoparticles of anatase and rutile in the aqueous phase. *J. Colloid Interface Sci.* **2011**, *363* (1), 84−91.
(21) Hunter, R. J. *Foundations of Colloid Science*; Clarendon Press: Oxford, U.K., 2001.
(22) Chen, K. L.; Elimelech, M. Interaction of fullerene (C_{60}) nanoparticles with humic acid and alginate coated silica surfaces: Measurements, mechanisms, and environmental implications. *Environ. Sci. Technol.* **2008**, *42* (20), 7607−7614.
(23) Sauerbrey, G. Verwendung von schwingquarzen zur wägung dünner schichten und zur mikrowägung. *Z. Phys. A: Hadrons Nucl.* **1959**, *155* (2), 206−222.
(24) Vittorias, E.; Kappl, M.; Butt, H.-J.; Johannsmann, D. Studying mechanical microcontacts of fine particles with the quartz crystal microbalance. *Powder Technol.* **2010**, *203* (3), 489−502.
(25) Fatisson, J.; Domingos, R. F.; Wilkinson, K. J.; Tufenkji, N. Deposition of TiO_2 nanoparticles onto silica measured using a quartz crystal microbalance with dissipation monitoring. *Langmuir* **2009**, *25* (11), 6062−6069.
(26) Tufenkji, N.; Elimelech, M. Deviation from the classical colloid filtration theory in the presence of repulsive DLVO interactions. *Langmuir* **2004**, *20* (25), 10818−10828.
(27) Chen, G.; Liu, X.; Su, C. Transport and retention of TiO_2 rutile nanoparticles in saturated porous media under low-ionic-strength conditions: Measurements and mechanisms. *Langmuir* **2011**, *27* (9), 5393−5402.
(28) Zhuang, J.; Qi, J.; Jin, Y. Retention and transport of amphiphilic colloids under unsaturated flow conditions: Effect of particle size and surface property. *Environ. Sci. Technol.* **2005**, *39* (20), 7853−7859.
(29) Thio, B. J. R.; Zhou, D.; Keller, A. A. Influence of natural organic matter on the aggregation and deposition of titanium dioxide nanoparticles. *J. Hazard. Mater.* **2011**, *189* (1−2), 556−563.
(30) Goharshadi, E. K.; Samiee, S.; Nancarrow, P. Fabrication of cerium oxide nanoparticles: Characterization and optical properties. *J. Colloid Interface Sci.* **2011**, *356* (2), 473−480.
(31) Keller, A. A.; Wang, H.; Zhou, D.; Lenihan, H. S.; Cherr, G.; Cardinale, B. J.; Miller, R.; Ji, Z. Stability and aggregation of metal oxide nanoparticles in natural aqueous matrices. *Environ. Sci. Technol.* **2010**, *44* (6), 1962−1967.
(32) Gregory, J. Approximate expressions for retarded van der waals interaction. *J. Colloid Interface Sci.* **1981**, *83* (1), 138−145.
(33) Gregory, J. Interaction of unequal double layers at constant charge. *J. Colloid Interface Sci.* **1975**, *51* (1), 44−51.
(34) Pomorska, A.; Yliniemi, K.; Wilson, B. P.; Shchukin, D.; Johannsmann, D.; Grundmeier, G. QCM study of the adsorption of polyelectrolyte covered mesoporous TiO_2 nanocontainers on SAM modified Au surfaces. *J. Colloid Interface Sci.* **2011**, *362* (1), 180−187.
(35) Shen, C.; Li, B.; Huang, Y.; Jin, Y. Kinetics of coupled primary- and secondary-minimum deposition of colloids under unfavorable chemical conditions. *Environ. Sci. Technol.* **2007**, *41* (20), 6976−6982.
(36) Lausmaa, J. *XPS Analysis of Coating on QCM Sensor*; SP Swedish National Testing and Research Institute: Boras, Sweden, 2006.
(37) Lin, S.; Cheng, Y.; Bobcombe, Y.; L. Jones, K.; Liu, J.; Wiesner, M. R. Deposition of silver nanoparticles in geochemically heterogeneous porous media: Predicting affinity from surface composition analysis. *Environ. Sci. Technol.* **2011**, *45* (12), 5209−5215.
(38) Bai, R.; Tien, C. Particle detachment in deep bed filtration. *J. Colloid Interface Sci.* **1997**, *186* (2), 307−317.
(39) Torkzaban, S.; Kim, H. N.; Simunek, J.; Bradford, S. A. Hysteresis of colloid retention and release in saturated porous media during transients in solution chemistry. *Environ. Sci. Technol.* **2010**, *44* (5), 1662−1669.
(40) Elimelech, M.; O'Melia, C. R. Kinetics of deposition of colloidal particles in porous media. *Environ. Sci. Technol.* **1990**, *24* (10), 1528−1536.
(41) Shellenberger, K.; Logan, B. E. Effect of molecular scale roughness of glass beads on colloidal and bacterial deposition. *Environ. Sci. Technol.* **2002**, *36* (2), 184−189.
(42) Johnson, W. P.; Ma, H.; Pazmino, E. Straining credibility: A general comment regarding common arguments used to infer straining as the mechanism of colloid retention in porous media. *Environ. Sci. Technol.* **2011**, *45* (9), 3831−3832.
(43) Bhattacharjee, S.; Ko, C. H.; Elimelech, M. DLVO interaction between rough surfaces. *Langmuir* **1998**, *14* (12), 3365−3375.
(44) Huang, X.; Bhattacharjee, S.; Hoek, E. M. V. Is surface roughness a "scapegoat" or a primary factor when defining particle-substrate interactions? *Langmuir* **2010**, *26* (4), 2528−2537.
(45) Yi, P.; Chen, K. L. Influence of surface oxidation on the aggregation and deposition kinetics of multiwalled carbon nanotubes in monovalent and divalent electrolytes. *Langmuir* **2011**, *27* (7), 3588−3599.
(46) Elimelech, M.; Gregory, J.; Jia, X.; Richard, A. W. *Particle Deposition and Aggregation: Measurement, Modelling and Simulation*; Butterworth-Heinemann: Oxford, U.K., 1995.
(47) Menachem, E. Kinetics of capture of colloidal particles in packed beds under attractive double layer interactions. *J. Colloid Interface Sci.* **1991**, *146* (2), 337−352.
(48) Jiang, X.; Tong, M.; Li, H.; Yang, K. Deposition kinetics of zinc oxide nanoparticles on natural organic matter coated silica surfaces. *J. Colloid Interface Sci.* **2010**, *350* (2), 427−434.
(49) Deonarine, A.; Lau, B. L. T.; Aiken, G. R.; Ryan, J. N.; Hsu-Kim, H. Effects of humic substances on precipitation and aggregation of zinc sulfide nanoparticles. *Environ. Sci. Technol.* **2011**, *45* (8), 3217−3223.